Research Article Vol. 4, No. 1 / January 2017 / Optica 31

Plasmon-exciton-polariton lasing

Mohammad Ramezani,[1] Alexei Halpin,[1] Antonio I. Fernández-Domínguez,[2] Johannes Feist,[2] Said Rahimzadeh-Kalaleh Rodriguez,[3] Francisco J. Garcia-Vidal,[2,4,6] and Jaime Gómez Rivas[1,5,7]

[1]FOM Institute DIFFER, P.O. Box 6336, 5600 HH Eindhoven, The Netherlands
[2]Departmento de Física Teórica de la Materia Condensada and Condensed Matter Physics Center (IFIMAC), Universidad Autónoma de Madrid, E-28049 Madrid, Spain
[3]Centre de Nanosciences et de Nanotechnologies, CNRS, Univ. Paris-Sud, Université Paris-Saclay, C2N - Marcoussis, 91460 Marcoussis, France
[4]Donostia International Physics Center (DIPC), E-20018 Donostia/San Sebastian, Spain
[5]Department of Applied Physics, Eindhoven University of Technology, P.O. Box 513, 5600 MB Eindhoven, The Netherlands
[6]e-mail: fj.garcia@uam.es
[7]e-mail: j.gomezrivas@differ.nl

Received 19 September 2016; revised 18 November 2016; accepted 20 November 2016 (Doc. ID 276191); published 22 December 2016

Metallic nanostructures provide a toolkit for the generation of coherent light below the diffraction limit. Plasmonic-based lasing relies on the population inversion of emitters (such as organic fluorophores) along with feedback provided by plasmonic resonances. In this regime, known as weak light–matter coupling, the radiative characteristics of the system can be described by the Purcell effect. Strong light–matter coupling between the molecular excitons and electromagnetic field generated by the plasmonic structures leads to the formation of hybrid quasi-particles known as plasmon-exciton-polaritons (PEPs). Due to the bosonic character of these quasi-particles, exciton-polariton condensation can lead to laser-like emission at much lower threshold powers than in conventional photon lasers. Here, we observe PEP lasing through a dark plasmonic mode in an array of metallic nanoparticles with a low threshold in an optically pumped organic system. Interestingly, the threshold power of the lasing is reduced by increasing the degree of light–matter coupling in spite of the degradation of the quantum efficiency of the active material, highlighting the ultrafast dynamic responsible for the lasing, i.e., stimulated scattering. These results demonstrate a unique room-temperature platform for exploring the physics of exciton-polaritons in an open-cavity architecture and pave the road toward the integration of this on-chip lasing device with the current photonics and active metamaterial planar technologies.

OCIS codes: (240.5420) Polaritons; (140.3460) Lasers; (250.5403) Plasmonics; (240.6690) Surface waves.

https://doi.org/10.1364/OPTICA.4.000031

1. INTRODUCTION

Exciton-polaritons—hybrid light–matter quasi-particles formed by strong exciton-photon coupling—have inspired more than two decades of highly interdisciplinary research [1]. Polariton physics has largely focused on semiconductor microcavities, where the strong nonlinearities associated with quantum well excitons [2,3] combined with the high quality factor cavities available through state-of-the-art epitaxial techniques have enabled the first observations of Bose–Einstein condensation (BEC) [4] and superfluidity [5] in optics. A key early vision of the field focused around the possibility of achieving a coherent light source at low threshold powers without the need for population inversion: a polariton laser [6]. Polariton lasers have remained in the realm of proof-of-principle experiments [7,8], and their widespread usage has not yet been adopted as efforts continue to lower thresholds and optimize operating parameters. In an effort to overcome some of the material-related limitations hampering applications of exciton-polaritons, as well as to explore novel light–matter states associated with distinct types of excitons, several researchers have recently turned their attention to organic materials [9–13]. While organic systems are generally disordered, their optical transitions can have large transition dipole moments, allowing them to couple strongly to light at room temperature. Several independent studies have already reported polariton lasing/BEC [14,15] and nonlinear interactions with organic excitons [16] in microcavities.

Recently, plasmonic systems have emerged as a promising alternative platform for exploring exciton-polaritons in an open architecture. The "cavity" defining the resonator is no longer a multilayer dielectric stack possessing a complex spectral response, and facilitates the integration of exciton-polariton devices with integrated photonics circuits. In these plasmonic systems, previously shown to be highly suitable for photon lasing [17–21], the excitonic material can be easily integrated by solution processing. The quality factors of plasmonic resonances are much lower than their counterparts in dielectric microcavities. However, the subwavelength field enhancements generated by resonant metallic nanostructures can significantly boost the light–matter coupling. Indeed, strong plasmon-exciton coupling has already been observed [11,13,22–27], but earlier attempts toward achieving

plasmon-exciton-polariton (PEP) lasing remained unsuccessful due to the inefficient relaxation mechanism of PEPs and the saturation of strong coupling at large pumping fluences [23]. Here, we demonstrate PEP lasing from an optically pumped array of silver nanoparticles coated by a thin layer of organic molecules at room temperature, occurring at a low threshold [8]. Strong coupling between excitons in the organic molecules and collective plasmonic resonances of the array forms PEPs. By increasing the PEP density through optical pumping, we observe a pronounced threshold in the emission intensity accompanied by spectral narrowing. Besides these generic lasing characteristics, our system exhibits two rather distinct features: first, the threshold power for PEP lasing is reduced in parallel with a degradation of the quantum efficiency of the material. This counterintuitive behavior, from the standpoint of conventional laser physics, is intimately related to the onset of strong coupling and the emergence of new eigenstates, i.e., PEPs. A second distinct feature of our PEP laser stems from the fact that the nanoparticle array supports dark as well as bright modes. The mode that first reaches the lasing threshold is in fact dark below the threshold. While dark-mode photon lasing has attracted significant interest in the plasmonics community for several years, we provide the first report of lasing from a dark mode in a strongly coupled plasmon-exciton system. Lasing from this dark (below threshold) mode also manifests in an abrupt polarization rotation of the emitted light by 90°-above threshold.

We first characterize strong coupling between excitons in an organic dye and the lattice modes supported by an array of silver nanoparticles through optical extinction measurements. Subsequently, using numerical and semi-analytical techniques, we analyze the modes supported by the array and the composition of the associated PEPs, respectively. Photoluminescence (PL) measurements on the sample pumped off-resonance provide the emission response at increasing PEP densities. At high emitter concentrations, we observe Rabi splitting, the signature of plasmon-exciton strong coupling, together with the appearance of stimulated scattering and PEP lasing. By measuring the dispersion of the PL at several pump fluences for both polarizations, we identify the dark mode responsible for PEP lasing in this system.

2. RESULTS AND DISCUSSION

Figure 1 shows the normalized absorption and PL spectra of a layer of PMMA doped with organic dye molecules. We use a rylene dye [N, N′-Bis(2,6-diisopropylphenyl)-1,7- and -1,6-bis (2,6-diisopropylphenoxy)-perylene-3,4:9,10-tetracarboximide] as an emitter [28], due to its high photostability and low propensity toward aggregation at high concentrations. Two distinct peaks corresponding to the main electronic transition at $E = 2.24$ eV and the first vibronic sideband at $E = 2.41$ eV are evident in the absorption spectra of the molecules. A layer of PMMA doped with dye molecules with a thickness of 260 nm is spin-coated on top of the plasmonic array of silver nanoparticles. An SEM image of the fabricated array is depicted in the inset of Fig. 1. The array consists of particles with dimensions of 200 nm × 70 nm × 20 nm, and the pitch sizes along the x and y directions are 200 and 380 nm, respectively.

First, we measure the angle-resolved extinction of the nanoparticle array when covered by an undoped layer of PMMA [Figs. 2(a) and 2(c)]. The polarization of the incident light is fixed and set to be either perpendicular (top row) or parallel (bottom row) to the long axis of the nanoparticles, as indicated by the arrow in the inset. Here, we take advantage of a particular type of plasmonic mode that is supported by periodic arrays of metal nanoparticles, the so-called surface lattice resonances (SLRs). These modes are the result of the radiative coupling between localized surface plasmon (LSP) resonances in the individual nanoparticles enhanced by the in-plane diffracted orders of the array, i.e., the Rayleigh anomalies (RAs). The energy dispersions and quality factors of these SLRs can be tailored by varying the geometrical parameters and energy detuning between RAs and LSP resonances [29,30]. In addition, the enhanced in-plane radiative coupling reduces the radiative losses associated with localized resonances [31], and the redistribution of the electromagnetic field around the particles also reduces Ohmic losses [32], creating narrow resonances with high quality factors [31,33,34].

By probing the sample under different polarizations and angles of incidence, we couple to several resonances with distinct electric field distributions and symmetries, depending on which RAs are probed. The resonance with parabolic dispersion in Fig. 2(a) demonstrates the combination of both strong extinction and narrow linewidth in SLRs, which results, in this case, from the enhanced radiative coupling of $(0, \pm 1)$ RAs to a dipolar LSP resonance supported by the individual nanoparticles (see below). Similarly, by rotating the polarizer and aligning the incident electric field along the long axis of the nanoparticles, we

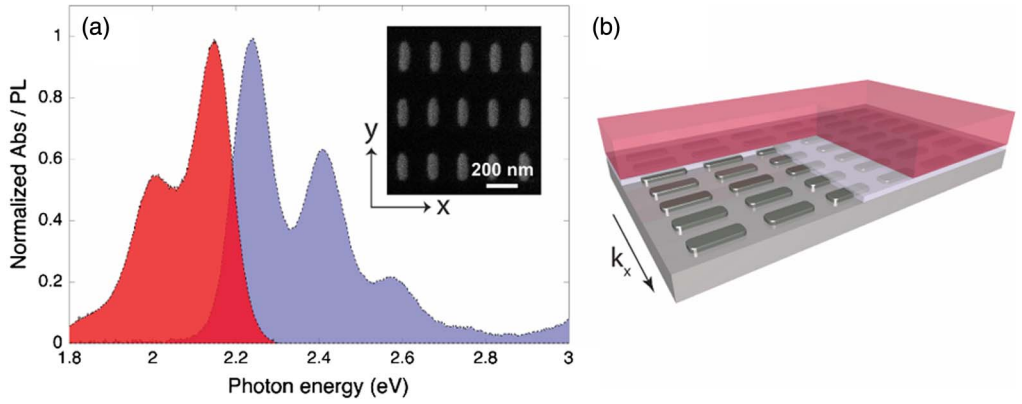

Fig. 1. (a) Normalized absorption (blue) and photoluminescence (red) spectra of the layer of PMMA doped with dye molecules in the absence of the plasmonic array. The inset shows an SEM image of the array of silver nanoparticles. (b) Schematic illustration of the array covered with a thin layer of PMMA doped with dye molecules.

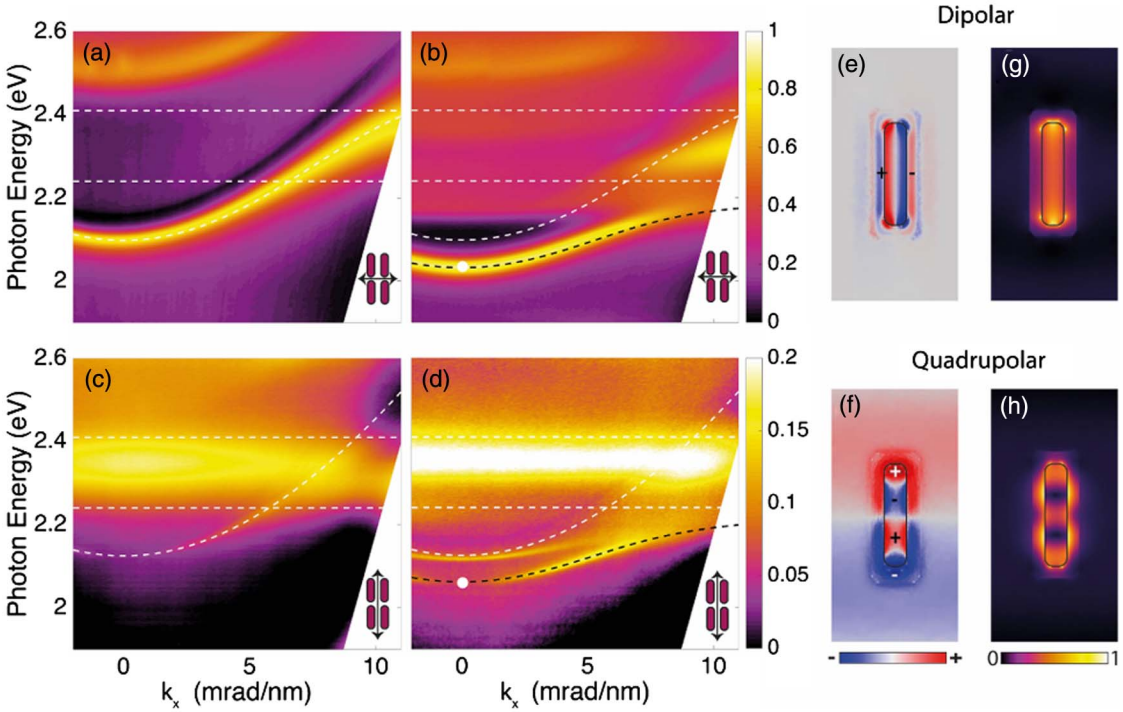

Fig. 2. Extinction measurements of the sample with incident light polarized along the short axis of the nanoparticles in the absence (a) and presence (b) of the dye molecules. The extinction of the same sample illuminated by light polarized along the long axis of the nanoparticles without (c) and with (d) the dye. The white dashed lines indicate the energies of the two strongest vibronic transitions in the molecules (horizontal lines) and the SLR dispersion, whereas the dashed black lines correspond to the lowest PEP modes. Maps of the induced charge density (e, f) and normalized electric field amplitude (g, h) for the corresponding lowest PEP modes at $k_x = 0$ mrad/nm. (e, g) correspond to the bright (dipolar-like) resonance, while (f),(g) to the dark (quadrupolar) resonance at $k_x = 0$ mrad/nm.

probe the coupling of $(0, \pm 1)$ RAs to a quadrupolar LSP resonance supported by the rods (see also below) [35]. Differences between the extinction measurements of Figs. 2(a) and 2(c) can be observed, where the most important is the vanishing SLR at $k_x = 0$ mrad/nm for the incident electric field parallel to the long axis of the rods. For this case, the electric field distribution is not dipole-active along the polarization direction. As a result, the coupling of the free-space radiation into this mode is inefficient, and the mode is dark at normal incidence. This behavior implies a strong reduction of radiation losses of this mode, which, as we will show later, is a key ingredient to achieve PEP lasing [36,37]. Due to the multipolar character of the dark mode, the net dipole moment is not zero (Fig. 2). This residual dipole moment is responsible for the out-coupling of the PL above the threshold that is reported below. Extinction measurements of the same array in the presence of a 260 nm thick PMMA layer doped with dye molecules are shown in Figs. 2(b) and 2(d). The dye concentration (C) in the polymer is 35 wt. %, and the measurements are referenced to the extinction of the doped layer without the nanoparticles. Increasing the molecular concentration modifies the extinction dispersion as a result of the hybridization between the SLR and the molecular transition. For both polarizations, we observe an anticrossing in the extinction dispersion and an associated Rabi splitting, $\hbar\Omega = 200$ meV, at $k_x \approx 7$ mrad/nm, which reveals the emergence of strong coupling between the SLR and molecular excitations. The coupling leads to the creation of upper and lower PEPs, where hybridization occurs for both the bright and dark modes. In Fig. 2(d), another resonance slightly blue-shifted with respect to the lower PEPs is visible. This resonance corresponds to the guided mode supported by the polymer layer. The appearance of this guided mode is due to the increase of the refractive index of the doped polymer layer when the molecular concentration is increased.

In order to analyze the hybrid light–matter nature of the PEPs formed by the strong coupling of the SLRs to the dye molecules, we use a few-level Hamiltonian that reproduces the measured extinction dispersions and allows the determination of the Hopfield coefficients defining the exciton and photon components of the strongly coupled system. We treat each field polarization separately, with the Hamiltonian (for each in-plane momentum)

$$H = \begin{pmatrix} E_{\mathrm{SLR}} & g_1 & g_2 \\ g_1 & E_{\mathrm{dye},1} & 0 \\ g_2 & 0 & E_{\mathrm{dye},2} \end{pmatrix},$$

where E_{SLR} is the energy of the SLR, $E_{\mathrm{dye},1}$ ($E_{\mathrm{dye},2}$) is the dispersionless energy of the first (second) absorption peak of the dye, and g_1 (g_2) describes the coupling between the SLR and the molecular modes. In Fig. 2, both the input energies of the "bare" states and the energy of the lowest PEP modes are depicted. As the actual system contains additional states at higher energies that we do not treat, we only show the lowest coupled state in the figure. From this analysis we can extract the Hopfield coefficients of the lower PEP, indicating that at $k_x = 0$ mrad/nm, it is composed of 75% SLR and 25% molecular excitations, with similar values obtained for both polarizations. We note here that while the SLR for the polarization along the long axis of the particles is dark

under far-field excitation at $k_x = 0$ mrad/nm, the coupling to the molecules occurs in the near field and thus attains similar strengths for both polarizations.

Electromagnetic calculations were also performed to simulate the extinction properties of the experimental samples. Both the finite-difference time-domain (FDTD) (Lumerical) and finite element method (FEM) (Comsol Multiphysics) methods were employed, finding an excellent agreement with the extinction maps in Fig. 2 (see Supplement 1 for details). Geometric and material parameters were extracted from SEM images of the samples and previously published literature [38], respectively. The right insets in Fig. 2 render the electric field amplitude and induced surface charge density maps evaluated at $k_x = 0$ mrad/nm. The top insets [Figs. 2(e) and 2(g)] show that, for a polarization along the short axis, the near field is governed by a bright dipolar-like LSP supported by rods, i.e., the so-called $(\lambda/2)$ LSP, as anticipated above. On the contrary, the bottom insets [Figs. 2(f) and 2(h)] indicate that a dark quadrupolar LSP, i.e., the $(3\lambda/2)$ LSP, resonates for incoming light polarized along the long axis of the rod. Importantly for lasing purposes, both polaritonic modes spectrally overlap within an energy window of a few meV. The vacuum Rabi frequency Ω defining the coupling strength is proportional to $\sqrt{N}$, where N is the number of excitons within the mode volume of the resonance. Therefore, achieving strong coupling with organic molecules requires increasing their concentration within the polymer matrix such that the exciton density is maximized [19,24,25]. However, one immediate drawback expected from increasing C for the emission is the emergence of considerable inter-molecular interactions, which can lead to spontaneous aggregation (modifying the spectral properties of the sample) and also to a reduction of fluorescence lifetime (τ) due to the enhancement of nonradiative decay channels (concentration quenching of the emission) [39]. Importantly, the dye molecules used here do not suffer from aggregation at high C, as the normalized absorption spectrum for different C remains unchanged (See Fig. S4 in Supplement 1 for details). To quantify the concentration quenching, we have measured the lifetime and quantum efficiency of the polymer layers at different C (see Supplement 1 for details). One can see that at low C, the quantum efficiency of the molecules is close to the unity and the lifetime of the excited molecules is 5.8 ns. However, by increasing C to 35 wt. %, the quantum efficiency is reduced to 3% with a corresponding reduction of the lifetime to $\tau = 400$ ps. The emissive properties of high C samples are thus unsuitable for stimulated emission and photon lasing, where a high quantum yield is desired for achieving gain. In fact, the prediction that lasing without inversion could be achieved by exploiting many-body coherence in strongly coupled exciton-photon systems has been a major motivation for the development of exciton-polariton lasers [6].

In order to investigate PEP lasing, we optically pump the sample nonresonantly and measure the PL spectra as a function of the incident excitation power for different concentration of the molecules. The wavelength of the pump laser is centered at $\lambda_{exc} = 500$ nm ($E_{exc} = 2.48$ eV), and the pump polarization is fixed along the short axis of the nanoparticles for all experiments. The spectra of the PL for the sample with $C = 35$ wt. % in the forward direction for different absorbed pump fluences is shown in Fig. 3(a), where we observe the appearance of a very sharp peak in the emission spectrum at a fluence of 18 $\mu J/cm^2$. In Fig. 3(b), we plot the maximum of the PL intensity as a function of the absorbed pump fluence for three different concentrations of dye. For the low concentration sample, $C = 15$ wt. %, the PL intensity increases linearly with the incident power. This sample is at the onset of the appearance of exciton-SLR hybridization in extinction (see Supplement 1). At $C = 25$ wt. %, we observe the emergence of a threshold in the PL, followed by a superlinear increase of the emission. The nonlinear response of the system is further increased at $C = 35$ wt. %, where the threshold fluence is lowered by a factor of 2. This threshold fluence is one of the lowest values observed in optically pumped organic polariton lasers [14–16] and also is lower than the reported threshold for plasmonic-based photon lasers in the weak coupling regime [20,40]. Note that in our experiments, photodegradation occurs before the transition to the weak coupling regime [23], so the appearance of photon lasing is precluded by the damage threshold. Moreover, it is interesting to note that below the threshold, the emission decreases as C increases. This decrease is mostly due to the reduction of the photoluminescence quantum yield (PLQE) (See Supplement 1).

The linewidth of the PL as a function of the absorbed pump fluence is shown in Fig. 3(c), where a strong reduction of the linewidth above the threshold and hence, a substantial increase of the temporal coherence, can be observed. In Fig. 3(d) we display the polarization of the emission below and above the threshold for the sample with $C = 35$ wt. %. Below the threshold, the emission of the sample is mainly polarized along the short axis of the particles, i.e., 90°. This emission is associated with PEPs originating from the hybridization of the bright SLR with excitons [see Fig. 2(b)]. Interestingly, above the threshold, the polarization of the emission rotates by 90° and is primarily oriented along the long axis of the particles. This polarization rotation strongly indicates that the emission above the threshold is dominated by the PEPs created from the dark modes whose polarizations oriented the long axis of the particles [see Fig. 2(d)].

After excitation, the molecules relax to the PEP band. In this incoherent relaxation, the in-plane momentum is not conserved, leading to a broad distribution of excitation across the whole band. Most of the excitation thus ends up in high-k_x reservoir modes that are almost uncoupled from the SLR [4]. In order to achieve polariton lasing, the population of a single state has to become large enough to obtain significant bosonic stimulation. In semiconductor microcavities, the necessary relaxation from the reservoir typically relies on exciton-polariton and polariton–polariton scattering. In contrast, microscopic models for organic polariton lasing have suggested that vibronic coupling can play a more important role for dissipating excess momentum than exciton-polariton and polariton–polariton scattering [41–43]. In this picture, high-frequency intramolecular vibrational modes allow exciton-polaritons to scatter directly from the reservoir toward the lower energy levels [44]. This implies that organic exciton-polariton lasing is most efficient when the relaxation from the reservoir to the lasing state is resonant with a strong optical phonon line [14]. As shown in the top inset of Fig. 3(a), this condition is exactly fulfilled in the current sample: the energy difference, $\Delta = \Delta_1 = \Delta_2$, between the vibronic subpeaks of the molecule (the phonon energy) corresponds exactly to the energy difference between the lowest peak and the lasing state. Moreover, one needs to take into account that in addition to the role of the lattice parameters in modifying the detuning between the SLR

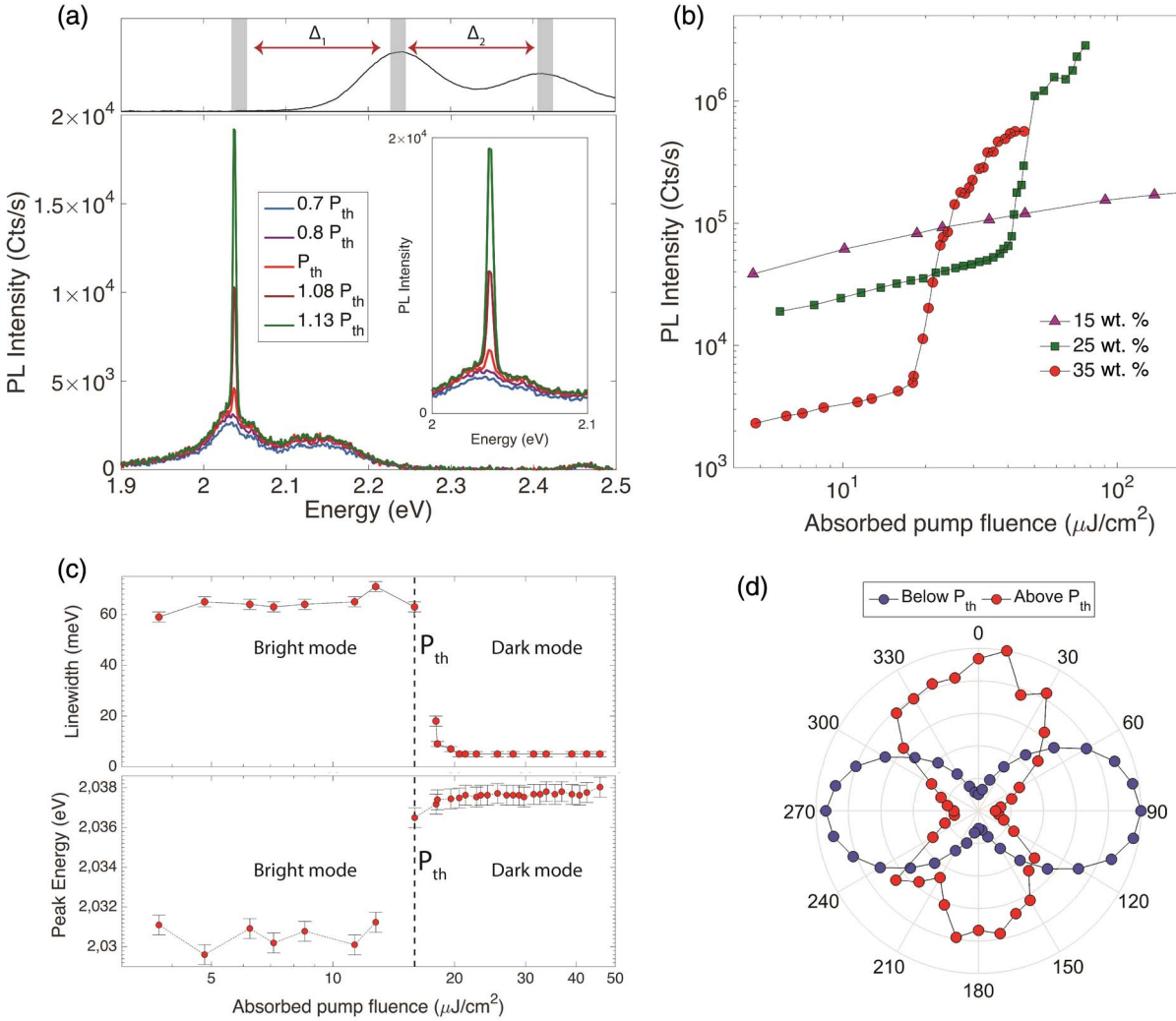

Fig. 3. (a) Emission spectra along the forward direction for the array of nanoparticles covered with PMMA with the dye concentration of 35 wt. % at increasing absorbed pump fluences. (Inset) Close view of the lasing peak. Upper panel: Absorption spectrum of the dye (solid curve). The energies of the lasing emission, the main electronic transition and the first vibronic side band of the molecule are indicated by the gray shaded areas. Note that the energy differences Δ_1 and Δ_2 are equal. (b) Photoluminescence peak intensity as a function of absorbed pump fluence for three samples at different dye concentrations. (c) Linewidth and energy shift of the photoluminescence peak as a function of absorbed pump fluence for the sample with $C = 35$ wt. % dye concentration. The linewidths and peak energies are extracted by fitting a Gaussian function to the spectrum. The error bars in the peak energy plot are set by the resolution of the spectrometer (≈1 meV) (d) Polarization of the emission from the sample with $C = 35$ wt. % below and above the threshold ($P = 1.5P_{\text{th}}$). The long axis of the nanoparticles is oriented along the vertical direction ($\theta = 0°$).

and the molecular exciton, the change of the molecular concentration can also alter the detuning through the change in the refractive index of the layer. The specific energy at which the polariton lasing occurs also poses an interesting question: while energy shifts are seen as the smoking gun for interactions between polaritons in semiconductor microcavities, the reported spectral behavior of polariton lasers in organic systems has been variable [14–16]. In our system, as the PLs below and above the threshold are dominated by different modes, we must distinguish the values of the energy shift for these two regimes. In Fig. 3(c), one can see that above the threshold, the dominant photoluminescence originating from the dark mode shifts by 1.3 meV and pins at 2.038 eV. Pinning of the energy shift above the threshold has been predicted by the model in Ref. [16]. This is in agreement with our measurements considering organic polariton interaction within the condensate.

Similar to the extinction measurements shown earlier, we can use angular-resolved measurements to study PEP emission at increasing pump fluences as we approach the critical density of PEPs [23]. In Fig. 4, we display the measured dispersion of the emission both below and above the threshold for two orthogonal detection polarizations corresponding to the bright and dark modes seen in Figs. 2(b) and 2(d). In Figs. 4(a) and 4(d), where the pump fluence is below the threshold, we recover the same dispersions as those shown previously in the extinction measurements, with a bright mode for the horizontal polarization and a dark mode for the vertical. We observe emissions over the whole range of k_x, indicating that, as mentioned above, the molecular relaxation process populating the PEPs after high-frequency excitation does not conserve $k_x = 0$ mrad/nm. Moreover, the PL from the uncoupled molecules lead to the green and cyan background in Figs. 4(a) and 4(d). Upon increasing the pump

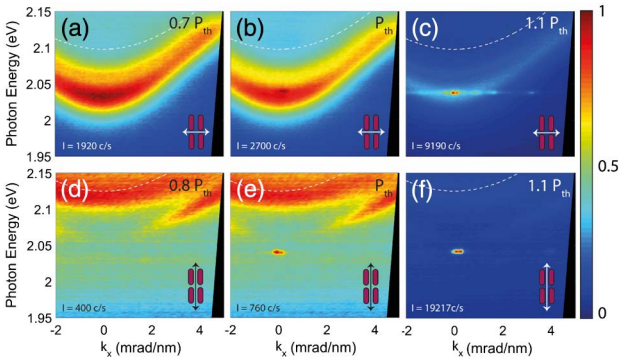

Fig. 4. Normalized angular-resolved emission measurements for two detection polarizations, parallel and orthogonal to the long axis of the nanoparticles, for the array of nanoparticles covered with PMMA with the dye concentration of 35 wt. %. The cartoon in the inset of each panel depicts the orientation of the nanoparticles with an arrow indicating the direction of the transmission axis of the polarization analyzer. The emission intensity in unit of counts/s at $E = 2.04$ eV and $k_x = 0$ mrad/nm for each detection condition is indicated at the bottom of each panel. (a)–(c) Angle-resolved PL for different pump fluences with the analyzer along the short axis of the nanoparticle visualizing to the bright mode along $(0, \pm 1)$ RAs supported by the array. (d)–(f) Angle-resolved PL for different pump fluences with analyzer along the long axis of the nanoparticle. In this configuration, the dark mode excited by $(0, \pm 1)$ RAs is probed. The bare modes associated with the uncoupled SLRs are shown by the white dashed line in each panel.

fluence, we observe a collapse in the emission pattern toward $k_x = 0$ mrad/nm over the narrow spectral range seen in the spectra of Fig. 3(a). As mentioned earlier, while the system exhibits no vertically polarized emission at normal incidence below the threshold, above the threshold, the lasing peak is mainly polarized along this direction. This behavior highlights one of the major differences between open systems defined by plasmonic lattices and traditional microcavities: the bright mode corresponding to the SLR of Fig. 2(a) represents a lossy mode due to the radiation losses, as it can efficiently couple out into free space. On the other hand, the dark mode is significantly less lossy at $k_x = 0$ mrad/nm due to the suppression of the radiation losses, which favors PEP lasing via this mode. The PEPs created via this mode can be accumulated with a much lower probability of decay. The energy dispersion of the bare modes associated with uncoupled SLRs for the dark and bright modes are shown in Fig. 4, indicating that the system remains in the strong coupling regime. We also observe, in Fig. 4(c), a residual PL emission with a flat dispersion at the energy in which the lasing occurs. This emission is most likely due to the scattering and polarization conversion of the PEP lasing emission from local imperfections in the sample.

3. CONCLUSION

In conclusion, we demonstrate the first polariton laser based on a plasmonic open cavity using an organic emitter. By exploiting diffractive coupling in a metallic nanoparticle array, we obtain spectrally sharp surface lattice resonance modes leading to the formation of PEPs in a dye-doped layer above the surface of the array. A lasing threshold in this system appears alongside the onset of strong coupling at high dye concentrations, when a sufficiently large number of molecules interacts with the SLR mode, leading to an avoided crossing, as seen in extinction measurements. At subsequently higher concentrations, the threshold pump energy diminishes, and we observe a very low lasing threshold in organic polariton laser systems. Though the observation of strong coupling appears in far-field measurements through the coupling of a bright mode to molecular resonances, the radiatively dark mode supported by the array plays a critical role in the near field, providing a low-loss channel in which polaritons can accumulate. This ultimately results in PEP lasing at an orthogonal polarization to that of the bright mode. While the optimal conditions for polariton lasing in plasmonic arrays remain to be determined, subsequent tailoring of both the mode structure of the array and the emitter could conceivably lower the lasing threshold reported here further (for instance, by making use of pump enhancement). Note that the energy difference between the RAs and the LSP resonance in arrays of nanoparticles defines the confinement of SLRs to the surface, i.e., the mode volume and also their quality factor, which affect the threshold. Therefore, arrays of metallic nanoparticles constitute a rich system that requires a thorough investigation. In addition, the ease of fabrication of large-area arrays by nanoimprint lithography and the open nature of the cavity opens a window through other interesting phenomena occurring in polariton systems with an architecture that provides potentially straightforward implementation into devices.

4. METHODS

A. Fabrication

The array of silver nanoparticles was fabricated by substrate conformal nanoimprint lithography following the procedure described in Ref. [45] on glass (Eagle 2000) and encapsulated by 8 nm of SiO_2 and 20 nm of Si_3N_4 to prevent the oxidation of the silver.

B. Characterization

The extinction measurements have been performed using a collimated polarized white light beam generated from a halogen lamp. The zeroth-order transmission of the white light from the sample under different incident angles ($T_0(\theta)$) was collected. For the reference measurement, the transmitted light through the same substrate and the polymer layer in the absence of the array ($T_0^{\mathrm{ref}}(\theta)$) is measured. The extinction is defined as $1 - T_0(\theta)/T_0^{\mathrm{ref}}(\theta)$.

All photoluminescence measurements except for the polarization measurement below the threshold in Fig. 3(b) have been done with amplified pulses generated from an optical parametric amplifier with an approximate pulse duration of 100 fs and a repetition rate of 1 kHz. Excitation using a low repetition rate but high pulse energies allows us to generate large densities of PEPs without the thermal damage associated with high-duty-cycle excitation. The excitation laser is focused on a 100 μm diameter spot on the sample. The polarization measurements below the threshold were done with a continuous-wave diode laser emitting at $\lambda = 532$ nm.

Funding. Nederlandse Organisatie voor Wetenschappelijk Onderzoek (NWO); Stichting voor de Technische Wetenschappen (STW); Philips; European Research Council (ERC) (290981); Seventh Framework Programme (FP7) (FP7-PEOPLE-2013-CIG-618229, FP7-PEOPLE-2013-CIG-630996); Spanish MINECO (MAT2014-53432-C5-5-R); Fundamental Research on Matter (FOM).

Acknowledgment. We sincerely thank Martin Könemann for providing us the organic dye. We are grateful to Marc A. Verschuuren for the fabrication of the samples.

See Supplement 1 for supporting content.

REFERENCES

1. C. Weisbuch, M. Nishioka, A. Ishikawa, and Y. Arakawa, "Observation of the coupled exciton-photon mode splitting in a semiconductor quantum microcavity," Phys. Rev. Lett. **69**, 3314–3317 (1992).
2. J. J. Baumberg, P. G. Savvidis, R. M. Stevenson, A. I. Tartakovskii, M. S. Skolnick, D. M. Whittaker, and J. S. Roberts, "Parametric oscillation in a vertical microcavity: a polariton condensate or micro-optical parametric oscillation," Phys. Rev. B **62**, R16247 (2000).
3. M. Saba, C. Ciuti, J. Bloch, V. Thierry-Mieg, and R. André, "High-temperature ultrafast polariton parametric amplification in semiconductor microcavities," Nature **414**, 731–735 (2001).
4. J. Kasprzak, M. Richard, S. Kundermann, A. Baas, P. Jeambrun, J. M. J. Keeling, F. M. Marchetti, M. H. Szymańska, R. André, J. L. Staehli, V. Savona, P. B. Littlewood, B. Deveaud, and L. S. Dang, "Bose–Einstein condensation of exciton polaritons," Nature **443**, 409–414 (2006).
5. A. Amo, J. Lefrère, S. Pigeon, C. Adrados, C. Ciuti, I. Carusotto, R. Houdré, E. Giacobino, and A. Bramati, "Superfluidity of polaritons in semiconductor microcavities," Nat. Phys. **5**, 805–810 (2009).
6. A. Imamoglu, R. Ram, S. Pau, and Y. Yamamoto, "Nonequilibrium condensates and lasers without inversion: exciton-polariton lasers," Phys. Rev. A **53**, 4250–4253 (1996).
7. S. Christopoulos, G. B. H. von Högersthal, A. J. D. Grundy, P. G. Lagoudakis, A. V. Kavokin, J. J. Baumberg, G. Christmann, R. Butté, E. Feltin, J.-F. Carlin, and N. Grandjean, "Room-temperature polariton lasing in semiconductor microcavities," Phys. Rev. Lett. **98**, 126405 (2007).
8. D. Sanvitto and S. Kena-Cohen, "The road towards polaritonic devices," Nat. Mater. **15**, 1061–1073 (2016).
9. D. G. Lidzey, D. Bradley, M. S. Skolnick, and T. Virgili, "Strong exciton–photon coupling in an organic semiconductor microcavity," Nature **395**, 53–55 (1998).
10. J. Bellessa, C. Bonnand, J. C. Plenet, and J. Mugnier, "Strong coupling between surface plasmons and excitons in an organic semiconductor," Phys. Rev. Lett. **93**, 036404 (2004).
11. J. Dintinger, S. Klein, F. Bustos, W. L. Barnes, and T. W. Ebbesen, "Strong coupling between surface plasmon-polaritons and organic molecules in subwavelength hole arrays," Phys. Rev. B **71**, 035424 (2005).
12. S. Kéna-Cohen, M. Davanço, and S. R. Forrest, "Strong exciton-photon coupling in an organic single crystal microcavity," Phys. Rev. Lett. **101**, 116401 (2008).
13. S. Aberra Guebrou, C. Symonds, E. Homeyer, J. C. Plenet, Y. N. Gartstein, V. M. Agranovich, and J. Bellessa, "Coherent emission from a disordered organic semiconductor induced by strong coupling with surface plasmons," Phys. Rev. Lett. **108**, 066401 (2012).
14. S. Kéna-Cohen and S. R. Forrest, "Room-temperature polariton lasing in an organic single-crystal microcavity," Nat. Photonics **4**, 371–375 (2010).
15. J. D. Plumhof, T. Stöferle, L. Mai, U. Scherf, and R. F. Mahrt, "Room-temperature Bose–Einstein condensation of cavity exciton-polaritons in a polymer," Nat. Mater. **13**, 247–252 (2013).
16. K. S. Daskalakis, S. A. Maier, R. Murray, and S. Kéna-Cohen, "Nonlinear interactions in an organic polariton condensate," Nat. Mater. **13**, 271–278 (2014).
17. R. F. Oulton, V. J. Sorger, T. Zentgraf, R.-M. Ma, C. Gladden, L. Dai, G. Bartal, and X. Zhang, "Plasmon lasers at deep subwavelength scale," Nature **461**, 629–632 (2009).
18. F. van Beijnum, P. J. van Veldhoven, E. J. Geluk, M. J. A. de Dood, G. W. t' Hooft, and M. P. van Exter, "Surface plasmon lasing observed in metal hole arrays," Phys. Rev. Lett. **110**, 206802 (2013).
19. J. Y. Suh, C. H. Kim, W. Zhou, M. D. Huntington, D. T. Co, M. R. Wasielewski, and T. W. Odom, "Plasmonic bowtie nanolaser arrays," Nano Lett. **12**, 1–6 (2012).
20. W. Zhou, M. Dridi, J. Y. Suh, C. H. Kim, D. T. Co, M. R. Wasielewski, G. C. Schatz, and T. W. Odom, "Lasing action in strongly coupled plasmonic nanocavity arrays," Nat. Nanotechnol. **8**, 506–511 (2013).
21. A. H. Schokker and A. F. Koenderink, "Lasing at the band edges of plasmonic lattices," Phys. Rev. B **90**, 155452 (2014).
22. T. K. Hakala, J. J. Toppari, A. Kuzyk, M. Pettersson, H. Tikkanen, H. Kunttu, and P. Törmä, "Vacuum Rabi splitting and strong-coupling dynamics for surface-plasmon polaritons and rhodamine 6G molecules," Phys. Rev. Lett. **103**, 053602 (2009).
23. S. R. K. Rodriguez, J. Feist, M. A. Verschuuren, F. J. Garcia-Vidal, and J. Gómez Rivas, "Thermalization and cooling of plasmon-exciton polaritons: towards quantum condensation," Phys. Rev. Lett. **111**, 166802 (2013).
24. S. Rodriguez and J. G. Rivas, "Surface lattice resonances strongly coupled to rhodamine 6G excitons: tuning the plasmon-exciton-polariton mass and composition," Opt. Express **21**, 27411–27421 (2013).
25. A. I. Väkeväinen, R. J. Moerland, H. T. Rekola, A. P. Eskelinen, J. P. Martikainen, D. H. Kim, and P. Törmä, "Plasmonic surface lattice resonances at the strong coupling regime," Nano Lett. **14**, 1721–1727 (2014).
26. E. Eizner, O. Avayu, R. Ditcovski, and T. Ellenbogen, "Aluminum nanoantenna complexes for strong coupling between excitons and localized surface plasmons," Nano Lett. **15**, 6215–6221 (2015).
27. G. Zengin, M. Wersäll, S. Nilsson, T. J. Antosiewicz, M. Käll, and T. Shegai, "Realizing strong light–matter interactions between single-nanoparticle plasmons and molecular excitons at ambient conditions," Phys. Rev. Lett. **114**, 157401 (2015).
28. M. Könemann, A. Bohm, N. Pschirer, J. Qu, and G. Mattern, "Substituted Rylene derivatives," U.S. patent US20080167467 A1 (July 10, 2008).
29. F. J. Garcia de Abajo, "Colloquium: light scattering by particle and hole arrays," Rev. Mod. Phys. **79**, 1267–1290 (2007).
30. A. Abass, S. R.-K. Rodriguez, J. G. Rivas, and B. Maes, "Tailoring dispersion and eigenfield profiles of plasmonic surface lattice resonances," ACS Photon. **1**, 61–68 (2014).
31. S. Zou, N. Janel, and G. C. Schatz, "Silver nanoparticle array structures that produce remarkably narrow plasmon lineshapes," J. Chem. Phys. **120**, 10871–10875 (2004).
32. K. Guo, G. Lozano, M. A. Verschuuren, and J. Gómez Rivas, "Control of the external photoluminescent quantum yield of emitters coupled to nanoantenna phased arrays," J. Appl. Phys. **118**, 073103 (2015).
33. A. D. Humphrey and W. L. Barnes, "Plasmonic surface lattice resonances on arrays of different lattice symmetry," Phys. Rev. B **90**, 075404 (2014).
34. G. Vecchi, V. Giannini, and J. Gómez Rivas, "Shaping the fluorescent emission by lattice resonances in plasmonic crystals of nanoantennas," Phys. Rev. Lett. **102**, 146807 (2009).
35. V. Giannini, G. Vecchi, and J. G. Rivas, "Lighting up multipolar surface plasmon polaritons by collective resonances in arrays of nanoantennas," Phys. Rev. Lett. **105**, 266801 (2010).
36. G. A. Turnbull, P. Andrew, M. J. Jory, W. L. Barnes, and I. D. W. Samuel, "Relationship between photonic band structure and emission characteristics of a polymer distributed feedback laser," Phys. Rev. B **64**, 125122 (2001).
37. A. B. Evlyukhin, C. Reinhardt, U. Zywietz, and B. N. Chichkov, "Collective resonances in metal nanoparticle arrays with dipole-quadrupole interactions," Phys. Rev. B **85**, 245411 (2012).
38. E. D. Palik, *Handbook of Optical Constants of Solids* (Academic, 2010).
39. J. R. Lakowicz, *Principles of Fluorescence Spectroscopy* (Springer, 2006), Vol. **3**.
40. T. P. H. Sidiropoulos, R. Roder, S. Geburt, O. Hess, S. A. Maier, C. Ronning, and R. F. Oulton, "Ultrafast plasmonic nanowire lasers near the surface plasmon frequency," Nat. Phys. **10**, 870–876 (2014).
41. L. Mazza, L. Fontanesi, and G. C. La Rocca, "Organic-based microcavities with vibronic progressions: photoluminescence," Phys. Rev. B **80**, 235314 (2009).
42. L. Mazza, S. Kéna-Cohen, P. Michetti, and G. C. La Rocca, "Microscopic theory of polariton lasing via vibronically assisted scattering," Phys. Rev. B **88**, 075321 (2013).
43. J. A. Ćwik, S. Reja, P. B. Littlewood, and J. Keeling, "Polariton condensation with saturable molecules dressed by vibrational modes," Europhys. Lett. **105**, 47009 (2014).
44. N. Somaschi, L. Mouchliadis, D. Coles, I. E. Perakis, D. G. Lidzey, P. G. Lagoudakis, and P. G. Savvidis, "Ultrafast polariton population build-up mediated by molecular phonons in organic microcavities," Appl. Phys. Lett. **99**, 143303 (2011).
45. M. A. Verschuuren, Substrate conformal imprint lithography for nanophotonics Ph.D. thesis (Utrecht University, 2010).